Density–functional theory study of stability and subgap states of crystalline and amorphous Zn-Sn-O

Wolfgang Körner[1,*] and Christian Elsässer[1,2]

[1]*Fraunhofer Institute for Mechanics of Materials IWM, Wöhlerstr. 11, 79108 Freiburg, Germany*
[2]*Institute for Applied Materials, Karlsruhe Institute of Technology, Kaiserstr. 12, 76131 Karlsruhe, Germany*

(Dated: May 1, 2013)

We present a density–functional theory analysis of stoichiometric and nonstoichiometric crystalline and amorphous Zn-Sn-O systems (c-ZTO, a-ZTO) which connects structural features with electronic properties in order to contribute to the understanding of the recently discovered subgap states in a-ZTO and other amorphous oxide films. In particular we show that defect levels originating from oxygen vacancies are too high in energy for being responsible for levels above the valence band edge. We offer an explanation for the experimentally seen decrease of subgap states with increasing oxygen content. From our analysis of the energetic stability of c- and a-ZTO compounds with different Zn/Sn ratios the decomposition of $ZnSnO_3$ into Zn_2SnO_4 and SnO_2 at sufficiently high temperatures is conceivable. Moreover, our results indicate that a lowering of the mass density of an a-ZTO sample leads to a rising of the conduction band edge.

PACS numbers: 64.70.kp,68.35.bj,72.80.Ng

I. INTRODUCTION

Amorphous oxide semiconductors begin to replace classical (poly-)crystalline transparent conducting oxides because they are easy and cheap to fabricate. Moreover they fulfill additional requirements for products such as organic light emitting diodes or rollable thin film transistor-liquid crystal displays on flexible substrates, namely uniform morphology and low deposition temperature (below 200°C). The multi-component amorphous oxide semiconductors In-Zn-O and In-Ga-Zn-O (IGZO) have attracted much attention since they show so far the best performances[1,2] concerning electrical conductivity and optical transparency. However, the Zn-Sn-O (ZTO) system is an attractive, cheap alternative since it is indium free and additionally provides good thermal stability, mechanical strength and good chemical stability under reducing atmosphere.[3–6]

In spite of the successful ZTO examples mentioned above various open questions remain. For instance: How is the band gap changing with the density or porosity of the amorphous structure? Several experimental groups have found that amorphous systems show similar or even bigger band gaps than their crystalline counterparts which contradict the common notion that disorder should reduce the band gap.[7–9]

What is the origin of the subgap states which for example play a role in thin film transistors ?[10] According to Ref. 1 and 11 the impact of disorder in amorphous oxide semiconductors on the conduction band (CB) edge is small since it mainly consists of metal s-states, whereas the valence band (VB) edge mainly consisting of direction dependent oxygen 2p states is strongly affected by structural disorder. They conclude that for amorphous oxide semiconductors the disorder leads to sharp CB tails whereas the VB tails are broad which apparently agrees with experimental findings (see e.g. the results of Erslev et al.[12] for a-$SnZnO_x$). However, the subgap states found in ZTO[12,13] and IGZO[10,14,15] are not covered by those general considerations on disorder. Theoretical investigations hint at localized defects, namely oxygen vacancies[16,17] and undercoordinated oxygen atoms[18], as possible sources of deep states above the VB.

In this paper we extend our analysis[18] of the origin of the subgap states for oxygen rich and oxygen poor amorphous Zn-Sn-O (a-ZTO) models. By claryfying the origin of the subgap states we can explain the experimentally seen decrease of subgap states by going to oxygen-rich conditions.[13]

A commonly done approach to answer questions like those posed above is the calculation of the density of states (DOS) of the c- and a-ZTO model systems with the local-density approximation (LDA) of the density functional theory (DFT). In our work, going beyond this, we

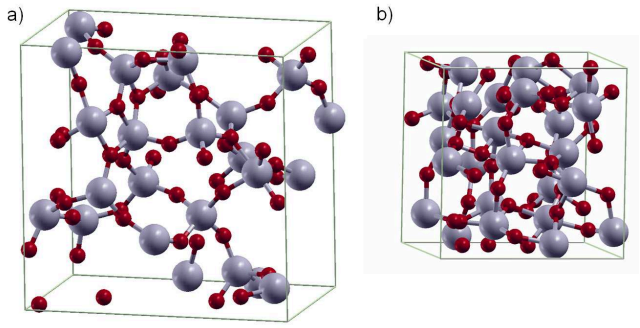

FIG. 1: (Color online) a) Supercell of sample E of set a-SnO_2(41%) with 102% volume increase with respect to c-SnO_2 and b) sample E of set a-SnO_2(16%) with 11% volume increase. Oxygen atoms are in red and Sn atoms in grey. In the amorphous sample of low density the Sn atoms are mostly tetrahedrally coordinated whereas in the amorphous sample of high density Sn atoms have mostly octahedral positions.

use a self-interaction correction (SIC) scheme for LDA since recent theoretical work[19–22] has shown that LDA has limited predictive power for wide band gap semiconductors due to its inherent artificial self-interaction. In addition to the DOS, we analyze the total energies of the c- and a-ZTO model systems to give answers to stability questions.

II. THEORETICAL APPROACH

A. SIC-LDA calculations

The total-energy and electronic-structure calculations in this work are performed on the basis of DFT using the computational mixed-basis pseudopotential method[24–27] with the same calculation setup as in our previous papers.[18–20] We have taken the LDA for exchange-correlation as parameterized by Perdew and Zunger.[28] For Zn, Sn and O optimally smooth norm–conserving pseudopotentials[30] are constructed, and a mixed–basis of plane waves and nonoverlapping localized orbitals are used. Due to the localized orbitals a plane–wave cutoff energy of 20 Ry (1Ry = 13.606 eV) is sufficient to obtain well converged results. For the k-point sampling of the Brillouin-zone integrals Monkhorst-Pack meshes of $3 \times 3 \times 3$ and a Gaussian broadening of 0.2 eV are used. The DOSs of the supercells were evaluated with the same mesh and a Gaussian smearing of 0.1 eV.

We solve the self-interaction problem of LDA (or generalized gradient approximation) by an implementation of the SIC in the pseudopotentials.[19,29] This does not increase the computational effort and thus is applicable to 100-atoms supercells. Our implementation uses a factor α measuring the deviation from the atomic SIC and weight factors w_i's accounting for occupation of the individual valence orbitals. All this is explained in detail in Ref. 19. For all oxides in this paper we used $\alpha = 0.8$. For c-ZnO and a-ZnO, correcting Zn 3d, O 2s and 2p, we used Zn(0, 0, 1) and O(1, 0.8, 0) where the bracket terms denote (w_0, w_1, w_2). Correspondingly, for SnO_2 in the rutile structure and a-SnO_2 we used Sn(0, 0, 1) and O(1, 0.93, 0). We had to modify the w_1 of oxygen accounting for the SIC of the 2p orbitals with respect to O potential of ZnO in order to reproduce the band gap for crystalline SnO_2. The main reason for the necessary adjustment is probably the change from fourfold tetrahedral coordination in the wurtzite structure of ZnO to sixfold octahedral coordination in the rutile structure of SnO_2. For all ternary Zn-Sn-O compounds we have chosen Zn(0, 0, 1), Sn(0, 0, 1) and O(1, 0.9, 0) which leads to an electronic band gap of 3.8 eV[18] for $ZnSnO_3$ which is well in the middle of the experimentally found 3.7 eV[31] and 3.9 eV.[32] In order to identify the energetic position of the various deep levels that appear in the DOS of a-ZTO samples we aligned the deep lying and well localized zinc 3d bands with the zinc 3d bands of the corresponding c-ZTO.

ion pair	A_{ij}(eV)	$\rho_{ij}(\AA)$	C_{ij}(eV·$\AA^6$)
Zn^{+2} – O^{-2}	499.3	0.3595	0.0
Sn^{+4} – O^{-2}	938.7	0.3813	0.0
O^{-2} – O^{-2}	22764.3	0.149	43.0

TABLE I: Buckingham potential parameters used for the molecular dynamics simulations taken from Ref. 23. Potential form: $V_{ij} = A_{ij} \cdot \exp(-r_{ij}/\rho_{ij}) - C_{ij} r_{ij}^{-6}$

B. Crystalline and amorphous Zn-Sn-O models

As reference and starting point for the generation of the amorphous model systems we constructed the following crystalline supercells ZnO(wurtzite-type, ($P6_3mc$), 72 atoms), c-Zn_2SnO_4 (inverse-Spinel-type[33]($P4_122$), and normal-Spinel-type (Fd3m), 56 atoms), c-$ZnSnO_3$ (Lithium-Niobate-type[34](R3c), and Ilmenite-type (R-3), 60 atoms) and hypothetical c-$ZnSn_2O_5$ (Pseudobrookite-type,[36](Cmcm), 64 atoms) and SnO_2 (rutile-type, ($P4_2mnm$) and α-quartz-type, ($P3_221$), 72 atoms). In the hypothetical α-quartz structure the Sn atoms are in tetrahedral position in contrast to the octahedral position in the real rutile structure which makes it a useful additional reference for low density a-SnO_2 in which the tetrahedral coordination dominates.

Following methodologically the pioneering work of Nomura et al.[35], we generated a-ZnO, a-Zn_2SnO_4, a-$ZnSnO_3$, a-$ZnSn_2O_5$ and a-SnO_2 structures by performing classical molecular dynamics (MD) with the GULP code.[38] Empirical interionic Buckingham potentials were employed whose rigid ion potential parameters are given in Table I. The MD started at 5000 K and was subsequently cooled down in steps of 10 K per ps with time steps of 2 fs at constant temperature and constant pressure.

For each Zn-Sn-O composition we generated a set of 5 *small* cells (denoted samples A − E) with the atom numbers of the above listed crystalline counterparts and a set of 3 *big* cells (448, 480 or 512 atoms). For each set we determined the radial distribution functions (RDFs) for all atom species and verified that the average RDFs of the small cells coincide well with the average RDFs of the big cells in order to exclude that the amorphous structures depend on the supercell sizes. Since for all compositions the RDFs of small and big supercells agreed (see Ref. 18 for a-$ZnSnO_3$ e.g.) we continued our analysis with the small cells which are tractable with DFT with reasonable computational effort. The small amorphous supercell models were then structurally relaxed using LDA by shifting the atoms according to the Broyden-Fletcher-Goldfarb-Shanno (BFGS) algorithm[37] until the residual forces on all atoms were less than 0.005 Ry/B_0 ($B_0 = 0.529\AA$).

For ZnO and SnO_2 we generated two further sets of 5 amorphous structures by MD simulations with the

initial temperature of 5000 K but with the constraint of constant volume(instead of constant pressure) in order to study the electronic structure of amorphous sets of different mass densities. We distinguish the sets of a-ZnO and a-SnO_2 by their average volume increase with respect to the single crystal written in brackets. We denote them by a-ZnO(8%)(constant pressure), a-ZnO(31%)(constant volume), a-SnO_2(16%)(constant volume) and a-SnO_2(41%)(constant pressure).

In order to study oxygen-poor and oxygen-rich amorphous structures we intrduced O, Zn or Sn vacancies. We generated 5 oxygen deficient, 5 zinc deficient and 5 tin deficient a-ZTO supercells by removing either an O, a Zn or a Sn atom from stoichiometric a-$ZnSnO_3$ supercells which we denote by a-$ZnSnO_3$:V_O, a-$ZnSnO_3$:V_{Zn} and a-$ZnSnO_3$:V_{Sn}(samples A − E). Following the example of Kamiya et al.[16] additional sets of 5 samples were created by melting the non stoichiometric structures at 5000 K and cooling them in steps of 10 K per ps with time steps of 2 fs at constant temperature and constant pressure. These samples in which the O, Zn and Sn holes are annihilated are denoted by a-$ZnSnO_3$:$V_{O(anh)}$, a-$ZnSnO_3$:$V_{Zn(anh)}$ and a-$ZnSnO_3$:$V_{Sn(anh)}$ (samples A − E).

III. RESULTS AND DISCUSSION

A. Atomic structures

The calculated structural parameters of the single crystals given in Table II deviate by less than 2 percent from experimental values. There exists no crystalline structure for $ZnSn_2O_5$. We have built $ZnSn_2O_5$ in the hypothetical Pseudobrookite(Cmcm) structure and check its energetic instability. Our optimized lattice parameters are a=3.92 $\AA$, b=10.19 $\AA$ and c=10.44 $\AA$. As additional reference for a-SnO_2 the hypothetical α-quartz structure($P3_221$) for SnO_2 was constructed in which the Sn atoms are in tetrahedral position. Our optimized lattice parameters are a=5.92$\AA$ and c=6.58$\AA$.

Table III contains the coordination numbers and mass densities of the c- and a-ZTO samples. The given values (some of these given in Ref. 18) for the amorphous compounds are the averages of the 5 samples generated per composition. The mass densities of the crystalline systems lie few percent above the experimental values due to the general underestimation of the lattice constants by the LDA. The average densities of the amorphous samples are about 10 to 50 percent lower than the crystal values which is seen also in experiments.[3,8,33,35]

The average coordination numbers of the amorphous samples given in Table III indicate the tendency of zinc and tin to prefer tetrahedral and octahedral coordination, i.e. having mostly 4-5 and 5-6 neighboring oxygen atoms, respectively. A notable exception is set a-SnO_2(41%) in which the tin atoms were predominantly in tetrahedral positions. This has an interesting influence on the electronic structure which is discussed below in Sec. III C 1. Oxygen has mostly tetrahedral coordination for high Zn content and trigonal or linear coordination for a-SnO_2 (see Fig. 1).

	ZnO	Zn_2SnO_4	$ZnSnO_3$	SnO_2
	wurtzite	inverse Spinel	lithium niobate	rutile
a	3.23 (3.258)[a]	8.62 (8.648)[b]	5.29 (5.262)[c]	4.81 (4.737)[d]
c	5.16 (5.22)[a]		14.11 (14.003)[c]	3.21 (3.19)[d]
u	0.38 (0.382)[a]		0.286 (0.2859)[c]	0.307 (0.307)[d]

TABLE II: Structure parameters calculated with LDA. The lattice parameters a and c are given in $\AA$ and the internal parameters u are dimensionless. Experimental values are given in brackets ([a] Ref. 42, [b] Ref. 33, [c] Ref. 34, [d] Ref. 43).

B. Formation energies

In Fig. 2 the formation energies in eV per formula unit (f.u.) of the considered crystalline and amor-

coordination numbers	Zn–O	Sn–O	O–O	O–(Zn, Sn)	ρ[g/cm^3]
a-ZnO(8%)	4.01		10.47	4.01	5.33
a-ZnO(31%)	3.62		8.26	3.62	4.01
c-ZnO ($P6_3mc$)	4		12	4	(5.60)[a] 5.81
a-Zn_2SnO_4	4.70	5.70	10.68	3.82	5.85
c-Zn_2SnO_4 ($P4_122$)	5	6	12	4	(6.42)[b] 6.50
a-$ZnSnO_3$	4.65	5.43	9.52	3.36	5.32
c-$ZnSnO_3$ (R3c)	6	6	12	4	6.76
a-$ZnSn_2O_5$	4.75	5.46	9.79	3.13	5.52
c-$ZnSn_2O_5$ (Cmcm)	5	6	10.4	3.6	6.09
a-SnO_2(16%)		5.62	10.18	2.81	5.61
a-SnO_2(41%)		4.42	7.48	2.21	3.95
c-SnO_2 ($P4_2mnm$)		6	13	3	(6.95)[c] 6.73

TABLE III: Coordination numbers and mass densities of the LDA-relaxed crystalline and amorphous model structures. The cut-off value was 3$\AA$ for Zn-O and Sn-O and 3.7$\AA$ for O-O. Experimental determined mass densities are given in brackets ([a] Ref. 8, [b] Ref. 33, [c] Ref. 39).

phous structures are depicted. The formation energies are given relative to the binary crystalline systems ZnO(wurtzite) and SnO_2(rutile): $E_{tot}(Zn_pSn_qO_{p+2q})$-$p{\cdot}E_{tot}(ZnO)$+$q{\cdot}E_{tot}(SnO_2)$ where E_{tot} denotes total energies determined with LDA. The conversion factor from eV/f.u to the experimentally more common kJ/mol is 96,35. We preferred a presentation of our results in eV/f.u since it simplifies the comparison to theoretical results of other groups.

Looking at Fig. 2 one notices that all considered ternary c-ZTO (with 2:1:4, 1:1:3 and 1:2:5 compositions) have positive energies meaning that they are only metastable. Although unexpected our results for the crystalline phases agree with previous calculations. For example the formation energies of the normal and the inverse spinel of c-Zn_2SnO_4 differ by 0.80 eV/f.u. which is close to the value of 0.68 eV/f.u. of Segev and Wei[40]. Also our results for c-$ZnSnO_3$ (R3c and R-3) agree very well with the results obtained by Gou et al. (see Fig. 3 of Ref. 41). Furthermore we agree with Gou et al.[44] that $ZnSnO_3$ in the R3c structure is energetically slightly lower than in the R-3 structure. Our value of 0.15 eV/f.u. is close to their 0.09 eV/f.u..

So far no crystalline phase for the 1:2 composition of Zn:Sn has been observed. The formation energy of the hypothetical Pseudobrookite c-$ZnSn_2O_5$(Cmcm) structure is lower than the formation energy of the amorphous samples of same composition however lies significantly above c-$ZnSnO_3$ (R3c and R-3), c-Zn_2SnO_4(inverse spinel) and the binary crystals. Thus it is likely to decay. Also our results are consistent with the observed decay of $ZnSnO_3$ into Zn_2SnO_4 and SnO_2 at high temperatures (about 600K).[44]

The amorphous structures have formation energies per f.u. of 0.2–2.0 eV, which is consistent with their observed metastability up to 450 °C.[13] and comparable to the theoretical values of about 1 eV obtained for IGZO.[17]

The green stars in Fig.2 indicate the formation energies of the samples of set a-ZnO(31%) and set a-SnO_2(41%). They have higher energies than their counterparts with lower volume a-ZnO(8%) and a-SnO_2(16%) (dark blue stars). The higher energy of the 5 amorphous samples of set a-SnO_2(41%) is caused by the tetrahedral-like coordinations of the Sn atoms. Their energies are spread around the c-SnO_2 (α-quartz-type,($P3_221$)) in which Sn is in perfect tetrahedral position. On average a higher volume and accordingly a lower coordination leads to higher energy of an amorphous sample. However, several of our samples with larger volume lie energetically lower than others with smaller volume since the total energy also depends on the contained point defects.

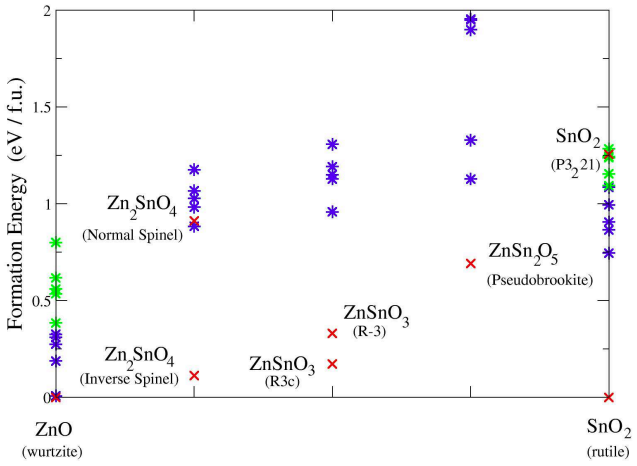

FIG. 2: (Color online) Total energy differences determined with LDA in eV per formula unit. The red crosses mark crystalyne phases. The dark blue stars mark amorphous structures. The green stars mark energies of the amorphous low density samples of set a-ZnO(31%) and set a-SnO_2(41%).

C. Electronic structure

1. *Stoichiometric ZTO*

In the upper part of Table IV the electronic band gaps of the c-ZTO structures determined with SIC (in brackets with LDA) and the experimentally measured gaps are listed. The lower part of Table IV contains the average band gaps of the a-ZTO structures and the average band tails at the VB and CB (some of these are given in Table II of Ref. 18). Additionally, the VB and CB edges of the stoichiometric c- and a-ZTO samples (ordered A to E) determined with SIC are depicted in Fig. 3.

The quantitative reduction of the band gap, determined with the SIC, of the a-ZTO samples compared to the c-ZTO counterparts is in line with the experimentally observed band gaps of 2.80 to 2.85 eV measured for a-ZTO by Jarayaj et al..[13] Looking at the tails of the band edges the SIC results show the expected behavior. The spherical s orbitals forming mainly the CB are rather insensitive to structural disorder and thus lead to small CB tails. The VB formed mainly of directional dependent O 2p orbitals and thus influenced more by disorder has significantly bigger tails in accordance with general theoretical considerations.[1,11] In contrast, LDA gives too narrow gaps, and also concerning the tails the LDA fails due to the self-interaction error in this approximation.

In Fig. 3 one can see that 9 of 10 CB edges of the high volume a-ZnO(31%) and a-SnO_2(41%) samples lie above their crystalline counterparts. In the a-ZnO(31%) samples the Zn atoms are mostly coordinated in planar oxygen triangles instead of tetrahedra and the Sn atoms in the a-SnO_2(41%) samples appear in tetrahedral instead of octahedral coordination (see Fig. 1). This fact is also

	$E_g^{SIC}(E_g^{LDA})$	E_g^{exp}	Space group
c-ZnO	3.23 (0.85)	3.40[a]	$P6_3mc$
c-Zn_2SnO_4	4.09 (1.52)	3.25-4.1[b]	$P4_122$
c-$ZnSnO_3$	3.80 (1.47)	3.7[c]-3.9[d]	R3c
c-$ZnSn_2O_5$	3.88 (1.40)		Cmcm
c-SnO_2	3.49 (1.36)	3.56[e]	$P4_2mnm$
	$E_g^{SIC}(E_g^{LDA})$	ΔE_{VB}^{SIC} (ΔE_{VB}^{LDA})	$\Delta E_{CB}^{SIC}(\Delta E_{CB}^{LDA})$
a-ZnO(8%)	2.65 (0.72)	0.56 (0.09)	-0.09 (-0.04)
a-ZnO(31%)	2.54 (0.81)	0.86 (0.12)	0.16 (0.09)
a-ZnO_2SnO_4	3.06 (0.88)	0.79 (0.30)	-0.24 (-0.34)
a-$ZnSnO_3$	2.61 (0.62)	0.86 (0.47)	-0.34 (-0.37)
a-$ZnSn_2O_5$	2.60 (0.74)	1.12 (0.38)	-0.16 (-0.28)
a-SnO_2(16%)	2.51 (0.57)	0.59 (0.32)	-0.38 (-0.45)
a-SnO_2(41%)	3.55 (1.40)	0.48 (0.46)	0.54 (0.50)

TABLE IV: Comparison of the electronic band gaps E_g determined using LDA and SIC-LDA ([a] Ref. 45, [b] Ref. 46 and references therein, [c] Ref. 31, [d] Ref. 32, [e] Ref. 47). All energies are given in eV. The values of the amorphous structures are the averages of the 5 samples per composition. ΔE_{VB}^{LDA}, ΔE_{CB}^{LDA}, ΔE_{VB}^{SIC} and ΔE_{CB}^{SIC} denote the average tail of the amorphous compounds compared to the crystalline structures. A negative value of ΔE_{CB}^{LDA} or ΔE_{CB}^{SIC} signifies a decrease of the CB edge whereas a positive value signifies that the CB edge moves up in energy. The error of the tails is about 0.05eV due to problem of alignment of the DOSs.

reflected in the coordination numbers for Zn-O and Sn-O given in Table III. The fact that the CB moves up for lower density is not an artefact of the SIC but is at least qualitatively in line with the LDA results. From Table IV one can see that also the LDA CB tails of a-ZnO(31%) and a-SnO_2(41%) are positive and not negative like for the case of smaller volume increase.

Further evidence that the upshift of the CB comes from the coordination of the metal atoms is provided by the model structure α-quartz SnO_2 in which all Sn atoms are tetrahedrally coordinated. We find with SIC a band gap of 4.60 eV which perfectly fits to the CB position of sample E of set a-SnO_2(41%) (see Fig. 1a) in which all Sn atoms are tedrahedrally coordinated as well. We conclude that the higher the degree of tedrahedral coordination and the lower the degree of octahedral coordination the bigger becomes the band gap.

The increased band gaps found experimentally in a-ZnO and a-SnO_2 samples[7–9] may be linked to the effect described above. However, the Burstein-Moss effect and quantum confinement phenomena induced by the nanoscopic size of crystallites may also contribute to the measured values.[8]

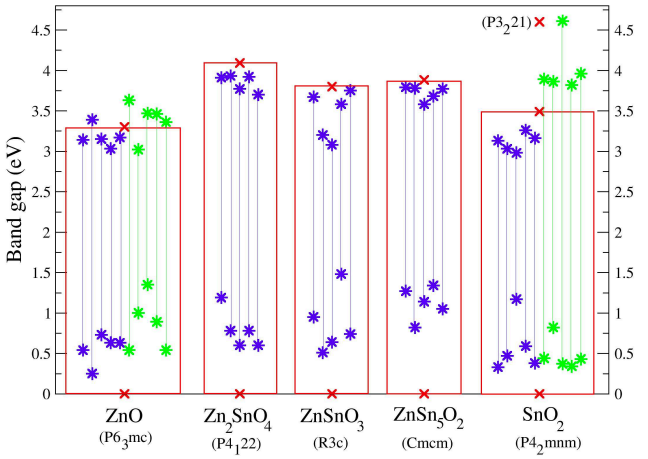

FIG. 3: (Color online) VB and CB edges of the stoichiometric c- and a-ZTO samples (ordered A–B, from left to right) determined with SIC. The CB edges of the ZTO crystals are set to zero. The green stars mark the VB and CB edges of the samples contained in a-ZnO(31%) and a-SnO_2(41%) which have high volume increases compared to the single crystals. For 9 out of 10 "high volume" samples the CB edge moves up.

2. *Oxygen poor ZTO*

Kamiya et al.[16] found in their LDA analysis for IGZO that oxygen vacancies (without subsequent amorphization step) form deep fully-occupied localized states near the VB maximum. If a subsequent amorphization step is included they find donor states at the CB minimum. Our LDA results for the DOS of a-ZTO fully agree with those findings for a-IGZO including the position of the Fermi level. However, due to the severe underestimation of the band gap in oxides those results have to be taken with caution. We don't present our LDA DOS here since they look very similar to those in the Figures 3 and 7 of Ref. 16 and continue with the discussion of the DOS obtained with the SIC which gives a more accurate and reliable picture.

Applying the SIC, all the oxygen poor a-$ZnSnO_3$ samples showed a VB tail of about 0.5 eV compared to the c-$ZnSnO_3$ similar to the stoichiometric structures (see Fig. 4). In addition to that disorder tail individual undercoordinated O atoms sometimes have even deeper levels of up to 1.3 eV. Compared to the stoichiometric a-$ZnSnO_3$ samples the oxygen poor a-ZTO samples have more and deeper levels below the CB. In Fig. 4 various samples having different defects are shown. Generally speaking, the deep levels lying deeper than 1.3 eV in the band gap originate from defects related to oxygen vacancies/deficiencies situated nearby one or two metal atoms. For comparison the neutral oxygen vacancy in c-ZnO lies at 2.2 eV[19] and in c-SnO_2 at 2.85 eV above the VB (both determined with SIC).

The label 1Sn in Fig. 4 denotes levels of one isolated Sn atoms surrounded by less than 6 O atoms. A sketch of

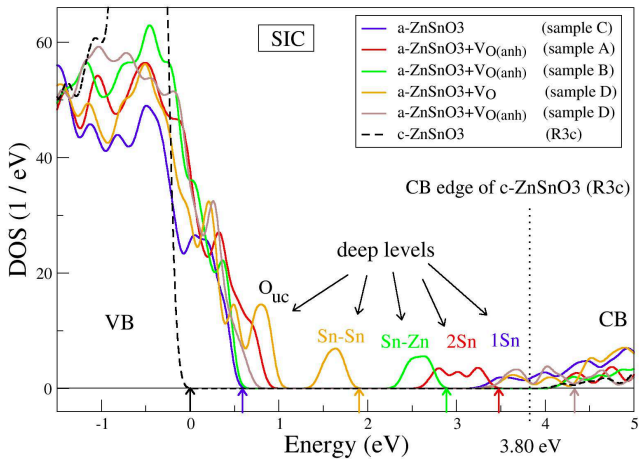

FIG. 4: (Color online) Total density of states of c-$ZnSnO_3$ and amorphous supercells which partially contain oxygen vacancies (V_O). The tails of about 0.5 eV width above VB originate from the O 2p disorder. Partially higher levels stem from undercoordinated oxygen atoms (O_{uc}). The deep levels lying higher in the gap originate from defects related to oxygen holes. Sn-Sn and Sn-Zn denote levels caused by two Sn atoms or a Sn and a Zn atom respectively. 1Sn and 2Sn denote levels of isolated Sn atoms surrounded by O atoms which strongly deviate from the perfect octahedra. The little arrows at the bottom mark the highest occupied levels of the DOS.

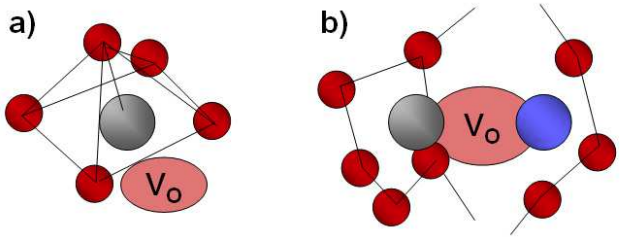

FIG. 5: (Color online) a) Sketch of a typical 1Sn defect. 1Sn defects consist typically of a Sn atom (grey) surrounded by 4 or 5 O atoms (red). The void near the Sn atom can be interpreted as one or two oxygen vacancies (V_O). b) Sketch of a Sn-Zn defect that is characterized by a Sn and a Zn atom (blue) which lie next to each other without any buffering O atom in-between. The Sn-Sn defect looks very similar but has a bigger void between the adjacent Sn atoms.

the atomic structure of such a defect is shown in Fig.5a). For such defects the deep levels are localized at Sn atoms with 4 or 5 nearest O atoms. These configurations can be seen as a strongly deformed $Sn+O_6$ octahedra with one or two oxygen vacancies lying nearby. 3 out of our 10 oxygen-poor samples have such 1Sn defects. Those defects already appeared in the stoichiometric samples and were also described in Ref. 18. They lead to high defect levels near the CB (see Fig. 4). By 2Sn we denote a pair of two 1Sn defects which lie at a distance of about 3.5–4$\mathring{A}$. 2 out of 10 of our supercells contain such 2Sn defects. The energetic position of the 2Sn defect levels is lower than those of the 1Sn defects.

The defect levels lying in the middle of the band gap are caused by defect complexes which we denote by Sn-Sn and Sn-Zn. They consist of two Sn atoms or a Sn and a Zn atom lying next to each other, without any bridging O atom in-between plus surrounding O atoms. A sketch of the geometry is given in Fig. 5b). Only one out of our 10 oxygen poor a-$ZnSnO_3$ samples contained a Sn-Sn defect. The two Sn atoms are at a distance of 3.16$\mathring{A}$. An analysis of the local DOS showed that the deep levels are localized at those two Sn atoms and neighboring O atoms. The Sn-Zn defect is the most frequent one and appears in 4 of our 10 samples. The Sn and Zn atoms are at a distances of 2.7–2.9 $\mathring{A}$. Also here the deep levels are localized at those two metal atoms and the neighboring O atoms. The shape and energetic position of the 1Sn, 2Sn and Sn-Zn defect levels shown in Fig. 4 can be seen as characteristic since the results of the various supercells vary very little (in the order of 0.2 eV).

Deep defect levels due to Zn-Zn pairs and single undercoordinated Zn atoms (1Zn defect) did appear neither in stoichiometric nor non-stoichiometric samples. As can be seen in Fig. 4 all the defect levels in the band gap are fully occupied. Thus in a neutral, oxygen-poor sample the Fermi level is given by the highest occupied defect level. According to our calculation the 1Sn defects are frequent defects and lead to Fermi levels up to 4.3 eV above the VB edge which would promote n-type conduction in a-ZTO. Since these defects have oxygen vacancies an increase of the transparency should be obtainable by annealing in oxygen rich atmosphere. Such a reduction of the subgab states and the opening of the band gap has been observed experimentally by Jayaraj et al..[13]

3. *Oxygen rich ZTO*

As oxygen rich samples we mean the a-$ZnSnO_3$:V_{Zn} and a-$ZnSnO_3$:V_{Sn} model structures which correspond to a surplus of one or two oxygen atoms per supercell. In contrast to our oxygen poor a-ZTO samples which show numerous deep defect levels almost all our oxygen rich samples show gaps without subgap states. Only 1 out of 20 samples has a Sn-Sn defect. Furthermore the width of the disorder tails of the oxygen rich samples are similar to widths of the stoichiometric amorphous models and the relative surplus of oxygen does not to lead to more deep levels above the VB edge caused by undercoordinated O atoms. Hence oxygen rich a-ZTO should be more transparent than oxygen-poor a-ZTO. This finding is in accordance with the experiments of Jayaraj et al.[13] who have seen a decrease of subgap states and an increase of the band gap when going to oxygen-rich conditions.

IV. SUMMARY AND CONCLUSIONS

In summary, we have studied the atomic structures, formation energies and electronic densities of states of stoichiometric and nonstoichiometric c- and a-ZTO models using a SIC-LDA approach. The energetic stability of c- and a-ZTO compounds with different Zn/Sn ratios was analyzed with respect to binary c-ZnO(wurtzite) and c-SnO_2(rutile) and leads to the conclusion that apparently all ternary composition in the Zn-Sn-O system are metastable in terms of total (internal) energies. Amorphous structures are on average higher in energy the lower their densities are. The experimentally observed decomposition of $ZnSnO_3$ into Zn_2SnO_4 and SnO_2 at sufficiently high temperatures is conceivable from Fig. 2.

Furthermore, our calculations indicate that the lower the mass density of an a-ZTO sample the higher is its conduction band. This correlation may partially explain that certain amorphous films showed higher band gaps than their crystalline counterparts. Concerning the subgap states, our SIC calculations lead to the interpretation that the experimentally found deep states[15] in between 0 and 1.5 eV are related to undercoordinated O atoms. This is at variance to the interpretation of Kamiya et al.[16] based on oxygen vacancies. As stated in Ref. 18 the assignment of undercoordinated O atoms is further supported by the fact that hydrogen doping suppresses those defect levels in accordance with experiments.[15] According to our analysis the subgap states in the upper part of the band gap between 1.3 eV and 3.8 eV are caused by oxygen vacancy related defects. Annealing in oxygen rich atmosphere will likely lead to their removal and result in an increase of the transparency which has already been shown in experimentally.[13]

V. ACKNOWLEDGMENTS

Financial support for this work was provided by the European Commission through contract No. NMP3-LA-2010-246334 (ORAMA).

* Electronic address: wolfgang.koerner@iwm.fraunhofer.de

[1] K. Nomura, H. Ohta, A. Takagi, T. Kamiya, M. Hirano and H. Hosono, Nature (London), **432**, 488 (2004).
[2] H. Yabuta, M. Sano, K. Abe, T. Aiba, T. Den, H. Kumomi, K. Nomura, T. Kamiya and H. Hosono, Appl. Phys. Lett. **89**, 112123 (2006).
[3] D. L. Young, H. Moutinho, Y. Yan and T. J. Couts, J. Appl. Phys., **92**, 310 (2002).
[4] T. Moriga, Y. Hayashi, K. Kondo, Y. Nishimura, K. Murai, I. Nakabayashi, H. Fukumoto and K. Tominaga, J. Vac. Sci. Technol. A, **22**, 1705 (2004).
[5] H. Q. Chiang, J. F. Wagner, R. L. Hoffman, J. Jeong and D. A. Keszler, Appl. Phys. Lett., **86**, 013503 (2004).
[6] J. H. Ko, I. H. Kim, D. Kim, K. S. Lee, T. S. Lee, B. Cheong and W. M. Kim, Appl. Surf. Sci., **253**, 7398 (2007).
[7] S. T. Tan, J. Chen, X. W. Sun, W. J. Fan, H. S. Kwok, X. H. Zhang and S. J. Chua, J. Appl. Phys., **98**, 013505 (2005).
[8] G. G. Valle, P. Hammer, S. H. Pulcinelli and C. V. Santilli, J. Europ. Ceram. Soc. **24**, 1009 (2004).
[9] J. M. Khoshman and M. E. Kordesch, Thin Solid Films **515**, 7393 (2007)
[10] H.-H Hsieh, T. Kamiya, K. Nomura, H. Hosono and C.-C. Wu, Appl. Phys. Lett. **92**, 133503 (2008).
[11] J. Robertson, Phys. Stat. Solidi. B **245**, 1026 (2009).
[12] P. V. Erslev, E. S. Sundholm, R. E. Presley, D. Hong, J. F. Wager and J. D. Cohen, Appl. Phys. Lett., **95**, 192115 (2009).
[13] M. K. Jayaraj, K. J. Saji, K. Nomura, T. Kamiya and H. Hosono, J. Vac. Sci. Technol. B **26**, 495 (2008).
[14] K. Nomura, T. Kamiya, H. Yanagi, E. Ikenaga and H. Hosono, Appl. Phys. Lett. **92**, 202117 (2008).
[15] K. Nomura, T. Kamiya, E. Ikenaga, H. Yanagi, K. Kobayashi and H. Hosono, J. Appl. Phys. **109**, 073726 (2011).
[16] T. Kamiya, K. Nomura, M. Hirano and H. Hosono, Phys. Stat. Sol. C **5**, 3098 (2008).
[17] T. Kamiya, K. Nomura and H. Hosono, Phys. Stat. Sol. A **206**, 860 (2009).
[18] W. Körner, P. Gumbsch and C. Elsässer, Phys. Rev. B **86**, 165210 (2012).
[19] W. Körner and C. Elsässer, Phys. Rev. B **81**, 085324 (2010).
[20] W. Körner and C. Elsässer, Phys. Rev. B **83**, 205306 (2011).
[21] P. Rinke, A. Janotti, M. Scheffler and C. G. Van de Walle, Phys. Rev. Lett. **102** , 026402 (2009).
[22] S. J. Clark, J. Robertson, S. Lany and A. Zunger, Phys. Rev. B **81**, 115311 (2010)
[23] G. V. Lewis and C. R. A. Catlow, J. Phys. C Solid State Phys., **18**, 1149 (1985).
[24] C. Elsässer, N. Takeuchi, K. M. Ho, C. T. Chan P. Braun and M. Fähnle, J. Phys.: Condens. Matter **2**, 4371 (1990).
[25] K. M. Ho, C. Elsässer, C. T. Chan and M. Fähnle, J. Phys. Condens. Matter **4**, 5189 (1992).
[26] B. Meyer, K: Hummler, C. Elsässer and M. Fähnle, J. Phys. Condens. Matter **7**, 9201-9217 (1995)
[27] F. Lechermann, M. Fähnle, B. Meyer and C. Elsässer Phys. Rev. B **69**, 165116 (2004).
[28] P. Perdew and A. Zunger, Phys. Rev. B **23**, 5048 (1981).
[29] D. Vogel, P. Krüger and J. Pollmann, Phys. Rev. B **54**, 5495 (1996).
[30] D. Vanderbilt, Phys. Rev. B **32**, 8412 (1985).
[31] H. Mizoguchi and P. M. Woodward, Chem. Mater. **16**, 5233 (2004).
[32] M. Miyauchi, Z. Liu, Z.-G. Zhao, S. Anandan and K. Hara, Chem. Commun. **46**, 1529 (2010).
[33] M.V. Nikolic, K. Satoh, T. Ivetic, K.M. Paraskevopoulos, T.T. Zorba, V. Blagojevic, L. Mancic, P.M. Nikolic, Thin Solid Films **516**, 6293 (2008)
[34] Y. Inaguma, M. Yoshida and T. Katsumata, J. Am. Chem.

Soc. **130**, 6704 (2008).
[35] K. Nomura, T. Kamiya, H. Ohta, T. Uruga, M. Hirano and H. Hosono, Phys. Rev. B **75**, 035212 (2007).
[36] Y. Suzuki and Y. Shinoda, Sci. Tech. Adv. Mater. 12, 034301(2011)
[37] W. H. Press, B. P. Flannery, S. A. Teukolsky and W. T. Vettering, *Numerical Recipies*, chapter 10.7., Cambridge (1986).
[38] J. D. Gale, J. Chem. Soc., Faraday Trans. **93**, 629 (1997).
[39] I. Saadeddin, H.S. Hilal, B. Pecquenard, J. Marcus, A. Mansouri, C. Labrugerea, M.A. Subramanian, G. Campet, Solid State Sciences **8**, 7 (2006)
[40] D. Segev and S.-H. Wei Phys. Rev. B **71**, 125129 (2005).
[41] H. Gou, J. Zhang, Z. Li, G. Wang, F. Gao, R. C. Ewing and J. Lian, Appl. Phys. Lett. **98**, 091914 (2011).
[42] F. Decremps, F. Datchi, A. M. Saitta, A. Polian, S. Pascarelli, A. Di Cicco, J. P. Itie and F. Baudelet Phys. Rev. B **68**, 104101 (2003).
[43] R. W. G. Wyckoff, *Crystal Structures*, 2nd ed. (Interscience, New York, 1963), p. 251
[44] H. Gou, F. Gao and J. Zhang, Comp. Mater. Sci. **49**, 552 (2010).
[44] D. Kovachera and K. Petrov, Solid State Ionics **109**, 327 (1998)
[45] M. Oshikiri and F. Aryasetiawan, Phys. Rev. B **60**, 10754 (1999).
[46] M. A. Alpuche-Aviles and Y. Wu, J. Am. Chem. Soc.**131**, 3216 (2009).
[47] D. Fröhlich, R. Kenklies and R. Helbig, Phys. Rev. Lett. **41**, 1750 (1978).